Tribology Letters (2025) 73:93
https://doi.org/10.1007/s11249-025-02023-x

ORIGINAL PAPER

Friction and Wear of PMMA Microspheres Rubbed Against Mo-Doped DLC Surfaces

Hesam Khaksar[1] · Hassan Zhairabany[2] · Chengfu Ma[3] · Liutauras Marcinauskas[2] · Enrico Gnecco[1]

Received: 12 March 2025 / Accepted: 9 June 2025

Abstract
The repeated rubbing of a polymer microsphere against a hard, nanorough surface is a paradigmatic and not-so-simple process in tribology. Here, we have investigated this process in the case of poly(methylmethacrylate) (PMMA) colloidal probes (15 μm diameter) elastically driven on a Mo-doped DLC film with RMS roughness of about 3 nm in ambient conditions. The probes are flattened on length scales of few tens of nm, increasing with the applied load (up to few tens of nN). A complementary analysis on a periodic silicon grating enables a quantitative characterization of the early-stage nanowear process. On the Mo-DLC film, two different contrasts are observed, corresponding to the probe forming a multi-contact interface with the rough surface or sliding across the top asperities of the film. The contact area between probe and film, in the multi-contact regime, is also estimated based on the Persson theory. It allows us to confirm that the flattening of the sphere must be limited, with the applied loading force values, to a contact radius of about 750 nm.

Keywords PMMA · Wear · Multicontact interface · Persson theory

1 Introduction

The sliding of polymers on hard surfaces is a problem of relevance in uncountable applications: industrial machinery (seals and gaskets, conveyor belts), biomedical applications (prosthetics and implants), transportation (automotive industry, rail and marine applications), packaging and consumer goods (household appliances, consumer products), energy sector (wind turbines and hydroelectric systems, oil and gas), additive manufacturing and prototyping (3D printing), aerospace and defense (structural components, lubrication-free bearings), electronics and robotics (wearable devices, robot components) [1]. In all these contexts, the unavoidable surface wear of the polymeric materials poses important questions not only on the efficiency and durability of the components, but also on implications on human health, with the most significant example being possibly the release of micro- and nanoplastics into the environment out of repeated surface scratching [2, 3]. For an effective mitigation of these problems, it becomes imperative to understand the dynamics of the sliding process, and specifically the complex relation between friction, wear and morphological properties of the sliding contact.

A very suitable characterization technique, in this context, is the so-called colloidal probe atomic force microscopy (CP-AFM) [4]. It is based on a spherical microsphere elastically driven on a surface with constant loading force and scan velocity. The friction between probe and surface is estimated from the torsion of the flexible cantilever, which is used to displace the sphere. In this way, the friction force is averaged all over the contact area established between probe and surface (with typical linear size in the order of tens of nm, see below). The spheres can be made of different materials, including polymers, and also coated with ultrathin films, which significantly increases the number of material combinations forming the sliding contact. In spite of these possibilities, friction force investigations based on CP-AFM are scarcely represented in the literature. Worth to note are a dedicated calibration method introduced by Varenberg et al. [5], lubricity effects observed when ionic liquids

✉ Enrico Gnecco
enrico.gnecco@uj.edu.pl

[1] M. Smoluchowski Institute of Physics, Jagiellonian University, ul. Łojasiewicza 11, Krakow, Poland

[2] Department of Physics, Kaunas University of Technology, Studentų str. 50, Kaunas, Lithuania

[3] State Key Laboratory of Solid Lubrication, Lanzhou Institute of Chemical Physics, Chinese Academy of Sciences, Lanzhou 730000, China

Published online: 27 June 2025

are confined between probes and rigid substrates [6], and original investigations of friction mechanisms on cellulose surfaces [7], polymer brushes [8] and tilted Ti nanorods [9]. When attempting to characterize friction with CP-AFM, the most obvious limitation is the occurrence of surface wear at the sliding interface. This effect is unavoidable when smooth and soft polymeric probes are rubbed on rougher and harder surfaces. Surface wear can be limited if the normal forces are kept in the nN range [10] or the probes are confined in surface valleys most of the time [11], but even in these cases the yield strength of the polymeric materials forming the probe (in the order of few tens of MPa) can be easily reached.

In this Letter, we have investigated the frictional behavior and the occurrence of surface wear in the exemplary case of a poly(methylmethacrylate) (PMMA) microsphere elastically driven on a nanorough Mo-doped DLC film and on an array of silicon spikes. They, respectively, represent surfaces with self-affine properties (in a well-defined range of length scales) and very regular (square) microtextures. In this way we aim to extend our current knowledge on a very basic microtribological mechanism, which can be useful not only for a fundamental understanding of the aforementioned problems, but also as a reference for applications to haptic sensors monitoring time variations of friction forces at different scales [12]. The Letter is divided as follows. We first demonstrate that the chosen Mo-doped DLC surface is self-affine in a range of length scales compatible with the maximum extension of the contact area established by the PMMA probe squeezed against it. Second, we distinguish two different regimes of motion: (i) sliding on a (variable) multiple asperity contact and (ii) "reverse stick–slip" across selected surface asperities (i.e.. the most protruding ones). The progressive wear of the PMMA probe suggested by the CP-AFM characterization of the Mo-doped DLC film is quantitatively demonstrated by the complementary analysis on the silicon grating, where the radius of curvature of the sphere getting blunt is precisely measured. Finally we show that the linear increase of friction with the loading force observed in the multiasperity contact regime is consistent with the predictions of the Persson contact theory applied to the nanorough film and the flattened PMMA sphere.

2 Materials and Methods

2.1 Mo-Doped DLC Surface

The Mo-doped DLC thin film was prepared by the DC magnetron sputtering technique. The film was grown using two flat magnetron targets (graphite and molybdenum) on silicon (100) substrates. Graphite (with a purity of 99.9%) and molybdenum (99.95% purity, from Testbourne suppliers) disc targets of 3-inch diameter were used. After pumping the chamber to a pressure of 10^{-2} Pa and before deposition, the cathodes were etched for 5 min in Ar plasma at a pressure of 2–3 Pa. The graphite target current was kept at 1.5 A and the Mo target current was fixed at 0.25 A during the deposition of the Mo-DLC films. The distance between the targets and the substrate was maintained at 8 cm. The deposition was carried out with Ar gas at 2–3 Pa pressure and the synthesis duration was kept at 600 s. The average thickness of the formed film was in the range of 150–160 nm. During deposition, the substrate holder moved parallel to the fixed target in a pendulum-like motion at a constant frequency of 0.3 Hz. As the substrate moved above the operating magnetron, multilayered carbon atoms were deposited on the substrate. A slit created on a shield was installed above the Mo target. The opening of this slit was used to gradually control the amount of Mo deposited in the samples [13]. The slit opening was maintained at 8 mm. The substrate temperature during film formation was increased and stabilized after 300 s. It was obtained that the temperature was about 185 °C ± 5 °C, when the Mo-DLC film was deposited.

Before detailing our CP-AFM characterization, we would like to stress the significance of Mo-DLC as a model system for nano-/microtribological studies beyond the topic addressed in this Letter. The incorporation of the molybdenum dopant in DLC coatings allows tuning the tribological behavior of the coating surfaces [13–16]. Indeed, we have recently shown that the microstructure and friction coefficient of the Mo-DLC films is significantly influenced by the Mo concentration [15]. Su Y. et al. [14] also found that the wear resistance is related to the linear size of the nanocrystals. Below 3 nm the adhesion and wear resistance improve due to the formation of a transfer layer containing MoO_2, which acts as a lubricating layer and reduces wear loss. The synthesis temperature plays also a crucial role and affects the surface tribology behavior by determining the amount of sp^2 or sp^3 carbon sites on the films. Last but not least, Hovsepian et al. [16] used the combination of Mo and W to prepare doped DLC coatings with improved tribological properties. The presence of the lubricious WS_2 and MoS_2 compounds was indeed found to maintain low values of the coefficient of friction ($\mu \sim 0.038$) at elevated temperature of 200 °C.

2.2 Colloidal-Probe Atomic Force Microscopy

The Mo-doped DLC surface was first imaged by AFM using qp-CONT probes (NanoAndMore, Germany) in ambient conditions. Lateral force (friction) measurements were performed with PMMA probes with diameter of 15 µm glued to silicon cantilevers with nominal resonance frequency of 13 kHz and spring constant of 0.2 N/m (CP-CONT-PM-E, NanoAndMore, Germany). To test the quality of the probes and provide the complementary characterization requested in our study, we have used a grating

consisting in a square array of sharp silicon tips with nominal radius of curvature below 10 nm and a 3 μm period (TGT1, NT-MDT Moscow, Russia). An AFM image of the grating is provided in Fig. 1a, whereas Fig. 1b gives an overview of the Mo-doped DLC film surface.

3 Results and Discussion

3.1 Self-Affine Properties of Mo-Doped DLC

The DLC film introduced in Sect. 2.1 has a RMS surface roughness $h_{\mathrm{rms}} = 3.13$ nm. The power spectral densities (PSD) of its height, $S(k)$, is plotted in Fig. 1c in a bi-logarithmic scale. Above the "roll-off" value $k_0 \approx 10^{7.3}$ m^{-1} the behavior is typical of self-affine surfaces [17]:

$$S(k) = S_0 \left(\frac{k}{k_0} \right)^{-2(H+1)} \tag{1}$$

The Hurst coefficient H in Eq. (1) is related to the fractal dimension D_f of the surface by the simple formula $H = 3 - D_f$. From the slope estimated in this range we obtain $D_f = 2.16$. Below k_0 the PSD fluctuates around a mean value S_0 given by the relation [18]

$$S_0 = \frac{H}{\pi \left[1 + H - \left(k_L / k_0 \right)^2 H \right]} \left(\frac{h_{\mathrm{rms}}}{k_0} \right)^2, \tag{2}$$

where $k_L = 6.3 \cdot 10^5$ m^{-1} is the wave number corresponding to the width $L = 10$ μm of the frame in Fig. 1b. With the values of h_{rms}, H and k_0 so determined we estimate $S_0 = 10^{-32.4}$ m^4. The characteristic length $\lambda_0 = 2\pi / k_0 = 0.31$ μm, quantifies the average size of the grains forming the surface.

3.2 CP-AFM on Mo-Doped DLC

Figure 2a shows an AFM topography of a different area of the Mo-doped DLC film, as obtained with the PMMA sphere with a normal force $F_N = 5$ nN. The surface appears as a random distribution of partially overlapping caps with diameter $2a \approx 1.5$ μm and radius of curvature $\rho \approx 115$ μm. As easily understood by a comparison with images taken on the grating (see below), the caps are artifacts caused by the convolution of the sphere with the top asperities of the surface [19]. A cross-section through the center of the circle highlighted by the green arrow is shown in Fig. 2b. Since the radius of curvature of the caps, ρ, is considerably larger than the original radius, $R = 7.5$ μm, of the sphere, the bottom of the last one must have been partially abraded while sliding against the DLC surface. From the sketch in Fig. 2c (not in scale), we can easily estimate that the caps have a height $h = \rho - \sqrt{\rho^2 - a^2} = 2.4$ nm. The radius of the sphere is therefore reduced by the quantity $R - \sqrt{R^2 - a^2} - h \approx 16$ nm, i.e., about 0.11% of R. Equivalently, a tiny fraction of 10^{-6} of the original volume of the sphere was removed.

The lateral force image acquired simultaneously to Fig. 2a is presented in Fig. 2d. From the cross-section corresponding to Fig. 2b and the lateral force signal acquired when the same line is scanned backward (Fig. 2e), it is visible that the average friction force (as estimated from half of the difference between the two curves) is considerably lowered when the probe is in contact with the top asperities of the Mo-doped DLC film. From the histogram of the lateral force values (Fig. 3a) we estimate that the friction is about 3 nN, and almost constant, when crossing individual asperities, whereas the average friction recorded on the whole image is about 15 nN. These measurements have been repeated, with a similar probe, with F_N varying between 2 and 14 nN. On a single asperity (Fig. 3b) the lateral force F_L is found to increase linearly with F_N. The "friction coefficient", as given

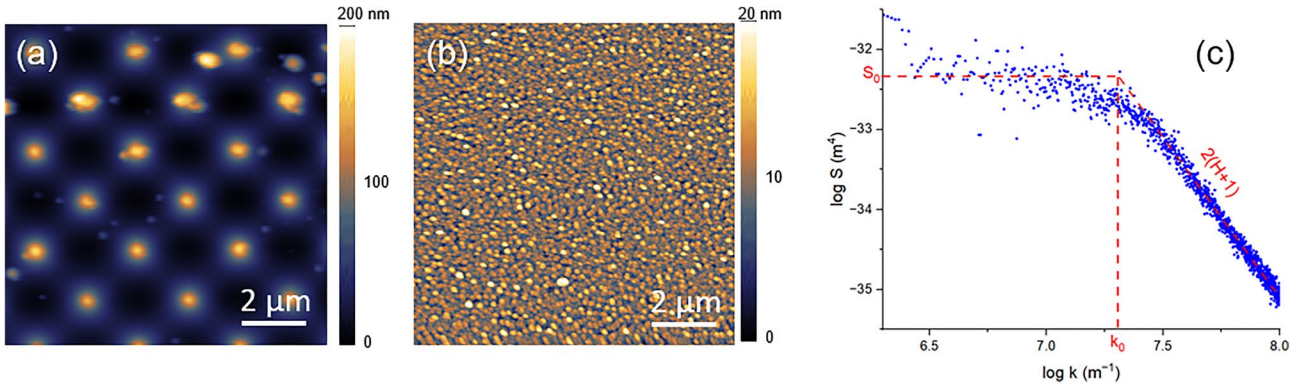

Fig. 1 **a** and **b** AFM topographies of the TGT1 grating and of the Mo-doped DLC film investigated in this work, respectively. **c** Power spectral density (PSD) of the image in (**b**)

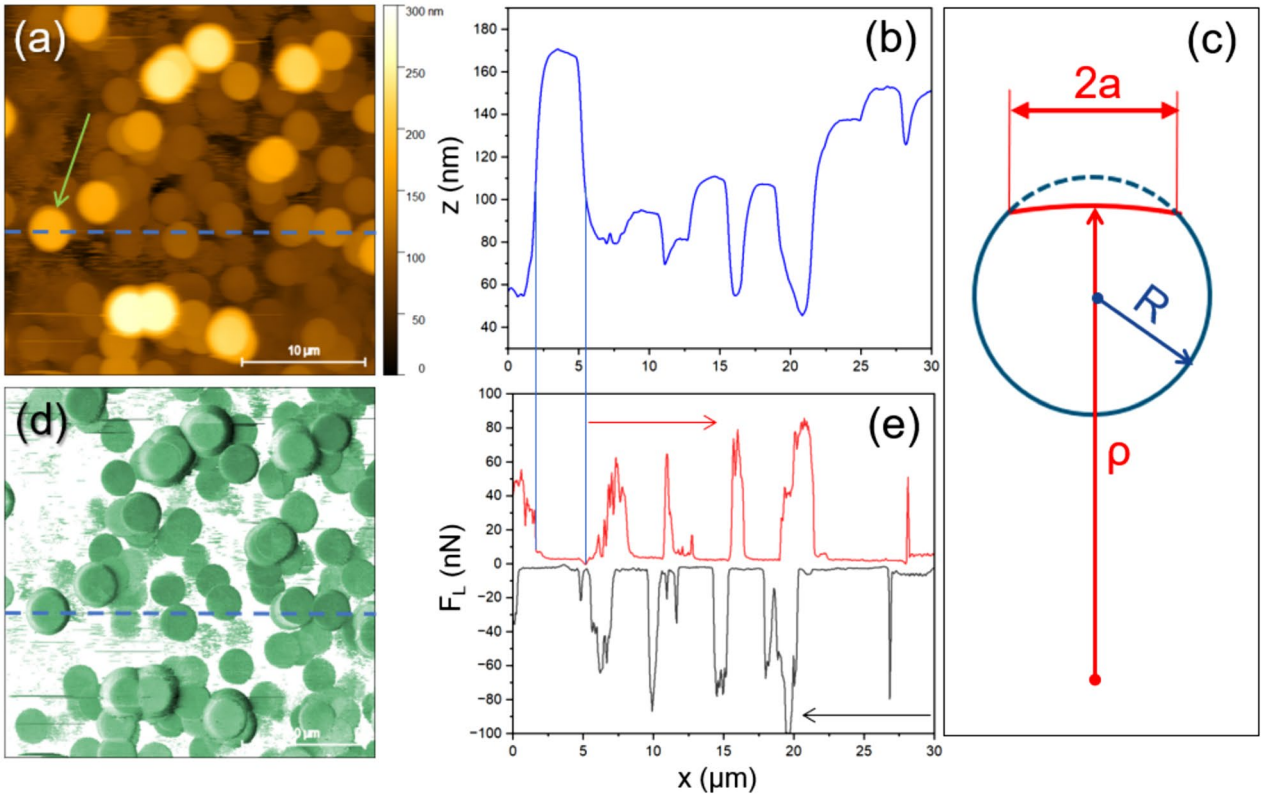

Fig. 2 **a** AFM topography of the Mo-doped DLC film as imaged with the colloidal PMMA sphere in contact mode (F_N=5 nN). **b** Cross-section corresponding to the dashed line in (**a**). **c** Sketch of the sphere before/after the wear test (not in scale). The circumference of the original probe is in blue. The repeated scratches result in the red arc. **d** Lateral force map simultaneously acquired with the topography. **e** Corresponding cross-section (red curve) together with the lateral force signal acquired backwards (black curve) (Color figure online)

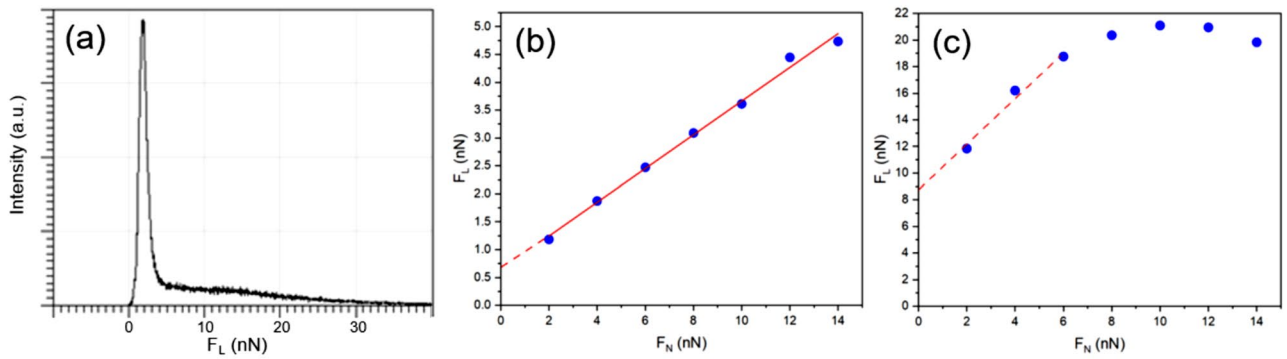

Fig. 3 **a** Lateral force histogram as obtained from the data in Fig. 2d. **b** and **c** Average lateral force values measured with the PMMA probe sliding across top asperities (corresponding to green circles in Fig. 2d) and, respectively, on the rest of the Mo-doped DLC film surface (Color figure online)

by the slope of the F_L vs. F_N curve, is μ=0.30. By prolonging the curve down to F_N=0, a residual lateral force F_0= 0.7 nN is estimated, which is due to the adhesion between the PMMA sphere and the doped Mo-DLC film. On the rest of the surface, where the probe is presumably in contact with several nanoasperities, the F_L vs. F_N curve is not linear (Fig. 3c). While the lateral force increases with a slope μ=1.4 in the very beginning, it curves towards a maximum at F_N=10 nN and even decreases slightly afterwards. The residual friction (for F_N=0) F_0 is about 9 nN. Interestingly, a similar trend has been recently reported in a theoretical work by Müller et al. and attributed to the elastic coupling

between normal and frictional interactions [20]. However, it must be noted that the authors addressed a complementary system (hard smooth surface vs. soft rough surface), which makes a quantitative comparison not feasible at the present stage.

3.3 CP-AFM on the Silicon Grating

For a better understanding of the surface wear of the PMMA sphere we have acquired several images of the silicon grating introduced in Sect. 2 with the normal force F_N increased stepwise from 10 to 80 nN. The selected images in Fig. 4a–c show that the sphere surface is smoothened as F_N increases. The radius of curvature ρ of the sphere has been estimated at the position highlighted by the green circle. As shown in Fig. 4d ρ is found to increase from 7.3 µm up to 29 µm. Note that the maximum value of ρ is lower than the value of 115 µm observed on the Mo-doped DLC film with a much lower value of $F_N = 5$ nN. As shown in Fig. 4e, the average friction was found to increase linearly on the grating (with $\mu = 0.25$) up to $F_N = 50$ nN and more rapidly up to $F_N = 80$ nN.

The lateral force maps corresponding to the sequence in Fig. 4a–c are shown in Fig. 5a–c. Horizontal cross-sections are shown in Fig. 5d. At the lowest value of $F_N = 10$ nN (black curve) the cross-section has a right-skewed shape. This is a manifestation of the so-called "reverse" stick–slip mechanism described by Özogul et al. for a similar PMMA sphere driven across a periodic grating [11]. When the sphere is driven across a spike the lateral force F_L, as measured by the cantilever torsion, *decreases* linearly with time, as described in [11] When a contact with the next spike is established, F_L suddenly *increases*, until the contact with the first spike is lost and the process repeats. As a result, the force profile caused by this mechanism shows the opposite trend of the standard stick–slip predicted e.g., by the Prandtl model for atomic-scale stick–slip [21]. For this reason, we address it with the term "reverse stick–slip" originally introduced by Lou et al. for the motion of a colloidal probe on an array of parallel nanotubes [22]. As shown in [11], the slope of the F_L vs. x curve in the stick phase is given by $S = (1 + \mu^2)F_N/R$, where μ is the coefficient of friction between PMMA and Si, and R is the radius of the probe. This is consistent with the value observed in Fig. 5d ($S = 0.0025$ N/m), with

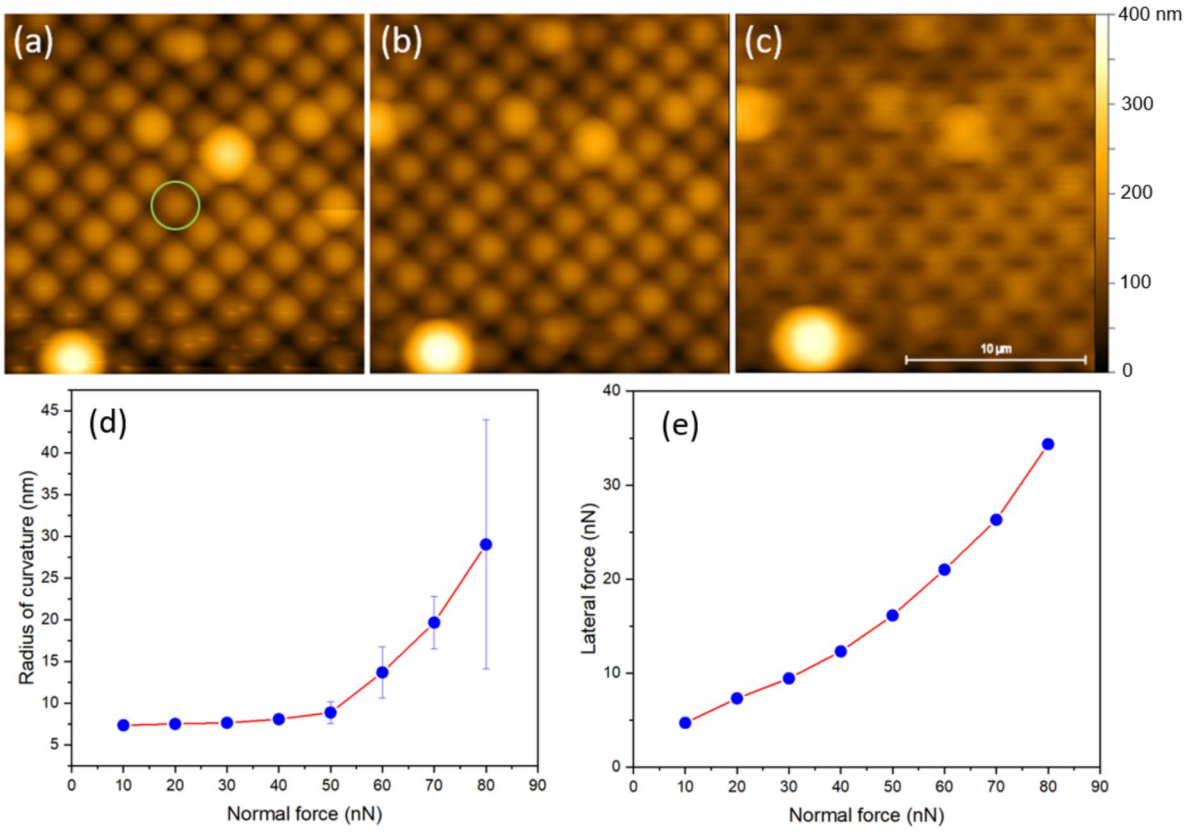

Fig. 4 **a–c** Topography maps of the TGT1 grating acquired with the PMMA probe and a normal force of 10, 40 and 70 nN. **d** Radius of curvature at the location highlighted by the green circle and **e** average friction force as a function of the loading force (Color figure online)

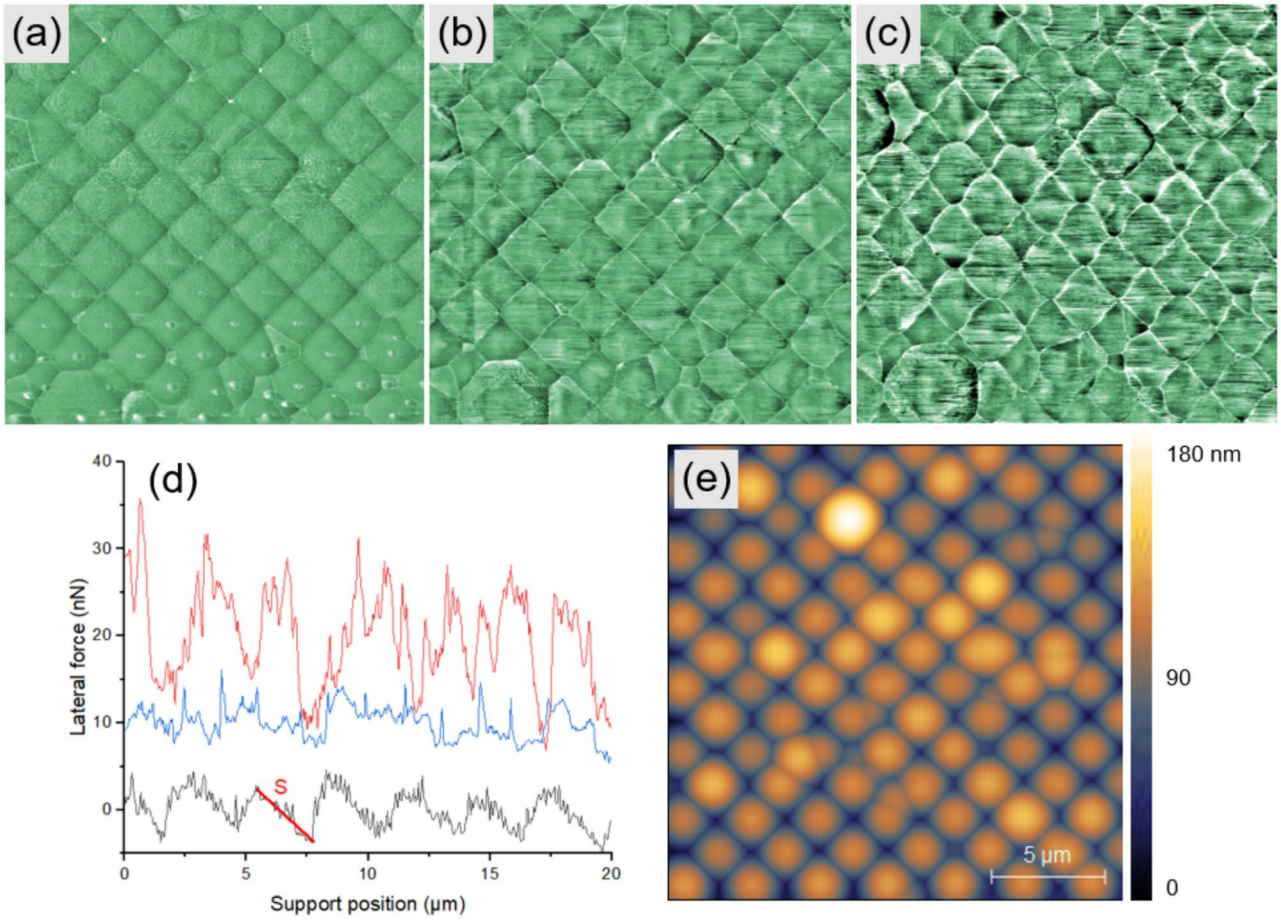

Fig. 5 **a–c** Friction maps recorded simultaneously with the colloidal probe AFM topographies in Fig. 4a–c. **d** Horizontal cross-sections corresponding to 10 nN (black), 40 nN (blue) and 70 nN (red). **e** Numerically processed convolution of a TGT-01 topography with a spherical virtual probe with diameter of 15 μm (Color figure online)

$\mu = 0.25$, provided that a pull-off force $F_{off} = 8$ nN is added to F_N. For comparison, the value of the coefficient of friction between PMMA and Si estimated in [11] was $\mu = 0.23$. It is also worth noting that, in the first scan lines the sphere surface is "cleaned" by the grating, as shown by the presence of bright dots that gradually disappear as the scan proceeds (see also [23]). Due to the small number and size of the spots, this effect is almost irrelevant in the estimation of the friction force. The situation is more complex when F_N increases. A comparison with Fig. 4 suggests that the sphere is still in contact with only one spike most of the time, except for the reverse slip phase. Nevertheless, the lateral force signal is significantly less regular, as compared to Fig. 5a. Abrasive/adhesive wear of the sphere surface is the most reasonable explanation for the observed features. As a result, the bottom of the sphere is irreversibly flattened, as shown from the larger radius of curvature of the probe observed when the load is brought back to its initial value.

It is also interesting to compare the image of the grating taken with a sharp tip (as zoomed in Fig. 1a) with a numerically processed image given by the geometric convolution of Fig. 1a with a rigid sphere with a given radius R. This has been done with the software WSxM 4.0 [24] with the result shown in Fig. 5e. From a comparison with the results in Fig. 4 it is apparent that the wider and brighter circles in Fig. 4a–c correspond to impurities sticking on the grating and protruding above the heights of the spikes.

3.4 Comparison with the Persson Contact Theory

According to the Persson theory, the contact area corresponding to a given value of the normal force, F_N, acting on a PMMA block squeezed against a rough surface is given by [25]

$$A(F_N) = A_0 \mathrm{erf} \frac{F_N}{2A_0\sqrt{G}}, \tag{3}$$

In Eq. (3) A_0 is the nominal contact area, $E^* = E/(1-\nu^2)$, where $E = 3$ GPa and $\nu = 0.37$ are, respectively, the Young's modulus and Poisson ratio of PMMA [26], and

$$G = \frac{\pi}{4} E^{*2} \int_{k_{\min}}^{k_{\max}} k^3 S(k) dk \tag{4}$$

The lower limit of integration, $k_{\min}$, is fixed by the nominal contact area $A_0 \approx 1.8 \times 10^{-12}$ m^2 corresponding to the circle with diameter $2a$ defined in Fig. 2c. Thus, $k_{\min} = 2\pi/a \approx 10^{6.9}$ m^{-1}. The upper limit of integration, $k_{\max}$, depends on the required level of magnification of the interface. With the dependence $S(k)$ estimated in Sect. 3.1 we obtain

$$G(k_{\max}) = \frac{\pi S_0 E^{*2}}{16}\left(k_0^4 - k_{\min}^4\right) + \frac{\pi S_0 E^{*2}}{8(1-H)k_0^{-2(H+1)}}\left(k_{\max}^{2(1-H)} - k_0^{2(1-H)}\right) \tag{5}$$

With the forces applied in our CP-AFM measurements, the force $F_N \ll A_0\sqrt{G}$. It implies that we can use the approximation $\mathrm{erf}(x) \approx 2x/\sqrt{\pi}$ and conclude from Eq. (3) that $A(F_N) \approx F_N/\sqrt{\pi G}$, or $F_L - F_0 = \mu F_N = \tau A$, where $\tau = \mu\sqrt{\pi G}$ is the interfacial shear stress between PMMA and the rough Mo-DLC surfaces. With the magnification in Fig. 2, $k_{\max} = 10^8$ m^{-1} and $\mu = 1.4$, $G = 1.85 \cdot 10^{16}$ Pa^2 and $\tau \approx$ 340 MPa. This value is above the shear strength of PMMA ($\tau_c = 100$ MPa) [22], meaning that smoothing of the PMMA probe at the lowest length scales is expected. The threshold value of $k_{\max}$, at which $\tau = \tau_c$, is $10^{7.4}$ m^{-1}. No significant damage is expected above the corresponding wave number $\lambda = 2\pi/k_{\max} \approx 250$ nm.

4 Conclusions

To sum up, we have investigated the motion of a colloidal PMMA sphere elastically driven on a rough Mo-doped DLC film (with self-affine properties above a certain wave number) and a periodic silicon grating. In the first case two sliding regimes are observed, corresponding to irregular multi-asperity contact and reverse stick–slip across the most prominent surface asperities. The presence of surface wear on the PMMA sphere is clearly visible on the Mo-DLC films. Its evolution is quantified by a series of curvature measurements on the grating. We have also applied the Persson contact theory to predict the maximum extent of the surface damage. Our results can be applied to fundamental investigations of tactility at the nano- to micrometer scale. Most important, we have shown that the unavoidable occurrence of surface wear of the polymeric unit can be maintained within acceptable limits if the normal force is kept well-controlled within a range of few tens of nN.

Author Contributions H. K. performed the AFM measurements and prepared the figures (with E. G.). H. Z. and L. M. prepared the Mo-DLC film investigated in the manuscript. E. G. interpreted the data, prepared the figures (with H.K.) and wrote the main manuscript C. M. supported the analysis based on the Persson theory. All authors reviewed the manuscript.

Funding H.K. and E.G. are thankful to the Strategic Program Excellence Initiative at the Jagiellonian University 'SciMat' (Grant No. U1U/P05/ NO/01.05). They also acknowledge the support of the Polish National Science Center (NCN) via the Opus Grant No. UMO/2021/43/B/ST5/00705. C.M. thanks the support by the National Natural Science Foundation of China (No. 52375556).

Data Availability Data sets generated during the current study are available from the corresponding author on reasonable request.

Declarations

Conflict of interest The authors declare no competing interests.

References

1. Sinha, S.K., Briscoe, B.J.: Polymer tribology. World Sci. (2009). https://doi.org/10.1142/p560
2. Sobhani, Z., Lei, Y., Tang, Y., Wu, L., Zhang, X., Naidu, R., Fang, C.: Microplastics generated when opening plastic packaging. Sci. Rep. **10**(1), 4841 (2020). https://doi.org/10.1038/s41598-020-61146-4
3. Hennig, J., Litschko, A., Mazo, J.J., Gnecco, E.: Nucleation and detachment of polystyrene nanoparticles from plowing-induced surface wrinkling. Appl. Surf. Sci. Adv. **6**, 100148 (2021). https://doi.org/10.1016/j.apsadv.2021.100148
4. Ducker, W.A., Senden, T.J., Pashley, R.M.: Measurement of forces in liquids using a force microscope. Langmuir **8**(7), 1831–1836 (1992). https://doi.org/10.1021/la00043a024
5. Varenberg, M., Etsion, I., Halperin, G.: An improved wedge calibration method for lateral force in atomic force microscopy. Rev. Sci. Instrum. **74**(7), 3362–3367 (2003). https://doi.org/10.1063/1.1584082
6. Espinosa-Marzal, R.M., Arcifa, A., Rossi, A., Spencer, N.D.: Ionic liquids confined in hydrophilic nanocontacts: structure and lubricity in the presence of water. J. Phys. Chem. C **118**(12), 6491–6503 (2014). https://doi.org/10.1021/jp5000123

7. Zauscher, S., Klingenberg, D.J.: Surface and friction forces between cellulose surfaces measured with colloidal probe microscopy. Nord. Pulp Pap. Res. J. **15**(5), 459–468 (2000). https://doi.org/10.3183/npprj-2000-15-05-p459-468
8. Bhairamadgi, N.S., Pujari, S.P., Leermakers, F.A., van Rijn, C.J., Zuilhof, H.: Adhesion and friction properties of polymer brushes: fluoro versus nonfluoro polymer brushes at varying thickness. Langmuir **30**(8), 2068–2076 (2014). https://doi.org/10.1021/la404915k
9. Datta, D., Gnecco, E., Gosvami, N.N., Singh, J.P.: Anisotropic stick–slip frictional surfaces via titania nanorod patterning. ACS Appl. Mater. Interfaces **16**(33), 44193–44201 (2024). https://doi.org/10.1021/acsami.4c06428
10. Cihan, E., Heier, J., Lubig, K., Gräf, S., Müller, F.A., Gnecco, E.: Dynamics of sliding friction between laser-induced periodic surface structures (lipss) on stainless steel and PMMA microspheres. ACS Appl. Mater. Interfaces **15**(11), 14970–14978 (2023). https://doi.org/10.1021/acsami.3c00057
11. Özoğul, A., Gräf, S., Müller, F.A., Gnecco, E.: Reverse stick-slip on a periodic wedge-shaped micrograting. Tribol. Lett.. Lett. **67**, 1–7 (2019). https://doi.org/10.1007/s11249-019-1139-x
12. Li, Y., Zhao, M., Yan, Y., He, L., Wang, Y., Xiong, Z., Wang, S., Bai, Y., Sun, F., Lu, O., Wang, Y., Li, T., Zhang, T.: Multifunctional biometic tactile system via a stick-slip sensing strategy for human-machine interactions, *NPJ Flex*. Electr. **6**, 46 (2022). https://doi.org/10.1038/s41528-022-00183-7
13. Su, Y., Gong, X., Huang, W., Zhang, T., Hu, R., Zhang, P., Ruan, H., Ma, Y.: Enhancing the tribological property of Mo-doped DLC films in methanol using appropriate bias voltage. Diam. Relat. Mater. **135**, 109795 (2023). https://doi.org/10.1016/j.diamond.2023.109795
14. Su, Y., Huang, W., Cai, L., Gong, X., Zhang, T., Hu, R., Zhang, P., Ruan, H.: Microstructural evolution and tribology of Mo-doped diamond like carbon nanocomposite film. Tribol. Int. **174**, 107774 (2022). https://doi.org/10.1016/j.triboint.2022.107774
15. Zhairabany, H., Dovydaitis, V., Khaksar, H., Vanags, E., Gnecco, E., Marcinauskas, L.: Influence of molybdenum concentration on the microstructure and nanotribological properties of diamond-like carbon films. J. Mater. Sci. **58**(33), 13437–13448 (2023). https://doi.org/10.1007/s10853-023-08854-0
16. Hovsepian, P.E., Mandal, P., Ehiasarian, A.P., Sáfrán, G., Tietema, R., Doerwald, D.: Friction and wear behaviour of Mo–W doped carbon-based coating during boundary lubricated sliding. Appl. Surf. Sci. **366**, 260–274 (2016). https://doi.org/10.1016/j.apsusc.2016.01.007
17. Berry, M.V., Lewis, Z.V., Nye, J.F.: On the Weierstrass-Mandelbrot fractal function. Proc. R. Soc. Lond. A **370**(1743), 459–484 (1980). https://doi.org/10.1098/rspa.1980.0044
18. Pastewka, L., Prodanov, N., Lorenz, B., Müser, M.H., Robbins, M.O., Persson, B.N.: Finite-size scaling in the interfacial stiffness of rough elastic contacts. Phys. Rev. E **87**(6), 062809 (2013). https://doi.org/10.1103/PhysRevE.87.062809
19. Villarrubia, J.S.: Algorithms for scanned probe microscope image simulation, surface reconstruction, and tip estimation. J. Res. Natl. Inst. Stand. Technol. **102**(4), 425 (1997). https://doi.org/10.6028/jres.102.030
20. Müller, C., Müser, M.H., Carbone, G., Menga, N.: Significance of elastic coupling for stresses and leakage in frictional contacts. Phys. Rev. Lett. **131**, 156201 (2023). https://doi.org/10.1103/PhysRevLett.131.156201
21. Prandtl, L.: Ein Gedankenmodell zur kinetischen Theorie der festen Körper. Z. Angew. Math. Mech. **8**, 85 (1928). https://doi.org/10.1002/zamm.19280080202
22. Lou, J., Ding, F., Lu, H., Goldman, J., Sun, Y., Yakobson, B.I.: Mesoscale reverse stick-slip nanofriction behavior of vertically aligned multiwalled carbon nanotube superlattices. Appl. Phys. Lett. **92**, 203115 (2008). https://doi.org/10.1063/1.2936866
23. Gan, Y., Franks, G.V.: Cleaning AFM colloidal probes by mechanically scrubbing with supersharp "brushes." Ultramicroscopy **109**(8), 1061–1065 (2009). https://doi.org/10.1016/j.ultramic.2009.03.019
24. Horcas, I., Fernández, R., Gomez-Rodriguez, J.M., Colchero, J.W.S.X., Gómez-Herrero, J.W.S.X.M., Baro, A.M.: WSXM: a software for scanning probe microscopy and a tool for nanotechnology. Rev. Sci. Instrum.Instrum. (2007). https://doi.org/10.1063/1.2432410
25. Yang, C., Persson, B.N.: Contact mechanics: contact area and interfacial separation from small contact to full contact. J. Phys. Condens. Matter **20**(21), 215214 (2008). https://doi.org/10.1088/0953-8984/20/21/215214
26. Protoxyz: Acrylic (PMMA). https://protoxyz.com/materials/plastic/Acrylic_(PMMA)